

An Angular-Temporal Interaction Network for Light Field Object Tracking in Low-Light Scenes

Mianzhao Wang, Fan Shi, Xu Cheng, Feifei Zhang, and Shengyong Chen, *Senior Member, IEEE*

Abstract—High-quality 4D light field representation with efficient angular feature modeling is crucial for scene perception, as it can provide discriminative spatial-angular cues to identify moving targets. However, recent developments still struggle to deliver reliable angular modeling in the temporal domain, particularly in complex low-light scenes. In this paper, we propose a novel light field epipolar-plane structure image (ESI) representation that explicitly defines the geometric structure within the light field. By capitalizing on the abrupt changes in the angles of light rays within the epipolar plane, this representation can enhance visual expression in low-light scenes and reduce redundancy in high-dimensional light fields. We further propose an angular-temporal interaction network (ATINet) for light field object tracking that learns angular-aware representations from the geometric structural cues and angular-temporal interaction cues of light fields. Furthermore, ATINet can also be optimized in a self-supervised manner to enhance the geometric feature interaction across the temporal domain. Finally, we introduce a large-scale light field low-light dataset for object tracking. Extensive experimentation demonstrates that ATINet achieves state-of-the-art performance in single object tracking. Furthermore, we extend the proposed method to multiple object tracking, which also shows the effectiveness of high-quality light field angular-temporal modeling.

Index Terms—Light field, Object tracking, Low-Light, Epipolar plane images.

I. INTRODUCTION

LIGHT field describes the geometric structural properties of light, encompassing both its propagation direction and intensity at each point in free space [1], [2], [3]. Existing vision model, such object trackers [4], [5], are typically developed based on RGB cameras that only use the intensity information of the light field. However, in complex scenarios such as low-light conditions, the intensity information of light is significantly weakened. 2D RGB images can only convey limited intensity information within the light field, leading to unsatisfactory tracking performance, as shown in Fig. 1(a). In such cases, the geometric structure information within the light field becomes particularly important, providing reliable discriminative features for the tracker, as shown in Fig. 1(b). Traditional imaging techniques utilize a main lens to capture the intensity of light converging onto a single point from multiple directions, forming a 2D image [6], [7]. However, these techniques inevitably result in the loss of geometric

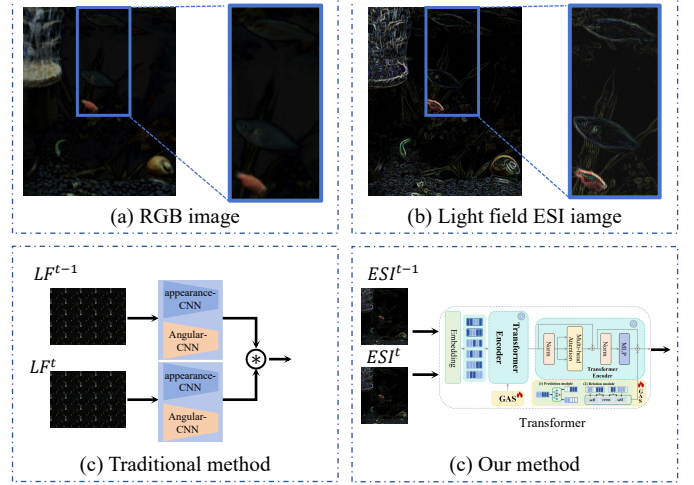


Fig. 1. The visual cues with different representations in low-light scenes and the comparison of existing methods for light field video feature extraction. (a) 2D RGB image from the center view. (b) Light field ESI representation. (c) Framework of traditional methods. (d) Framework of our proposed method.

structural information related to the light. In contrast, light field imaging technology captures structured light fields in a single shot using an array of micro-lenses, simultaneously recording both the intensity information in the spatial domain and the geometric structural information in the angular domain [8], [9]. The additional geometric information within the light field has shown tremendous potential in various computer vision applications, including depth estimation [10], [11], saliency detection [1], [12], and semantic segmentation [13]. These unique advantages of light field imaging have motivated further exploration of object tracking in low-light scenarios, expanding its applicability to video tasks. Therefore, in this paper, we aim to develop a light field object tracking framework. This framework is designed to extract light field features across angular and temporal dimensions, thereby enhancing the discriminative representations in low-light scenes.

In a light field imaging system, the captured structured light field video can be defined as $L(u, v, x, y)$, where (u, v) represents the angular coordinate system, and (x, y) represents the spatial coordinate system [14], [15]. Fixing two angular coordinates implies observing the scene from a specific angular domain, resulting in a general sequence of two-dimensional images [13]. On the other hand, fixing one angular coordinate and one spatial coordinate means gathering pixels from different angular domains, forming a sequence of epipolar plane images (EPIs) [16]. EPIs provide a structured representation

Corresponding author: Fan Shi, Xu Cheng.

Mianzhao Wang, Fan Shi, Xu Cheng, Feifei Zhang, Shengyong Chen are with the Engineering Research Center of Learning-Based Intelligent System (Ministry of Education), the key Laboratory of Computer Vision and System (Ministry of Education), Tianjin University of Technology, Tianjin, 300384, China (e-mail: wmz@stud.tjut.edu.cn, shifan@email.tjut.edu.cn, xu.cheng@ieee.org, feifeizhang@email.tjut.edu.cn, sy@ieee.org).

of the high-dimensional light field, revealing the geometric structural properties of the light field [11], [17]. Therefore, the light field encapsulates not only appearance and texture details in the spatial domain but also conveys geometric structural information across the angular and temporal domains, contributing to a more comprehensive understanding in low-light scenes. However, due to the high-dimensional structure of the light field, the angular domain tightly couples redundant appearance cues while sparsely distributing geometric structural cues. Although EPIs showcase the distribution of geometric structural cues in the angular domain by rearranging multi-view pixels [18], these representations still include redundant appearance cues, limiting the expressive capacity of light fields in the angular domain. Additionally, this redundant coupling necessitates the design of task-specific angular modules to explore geometric structural cues in the angular domain [19], as shown in Fig. 1(c), which in turn reduces the learning performance of the model. Therefore, decoupling the geometric structural cues of the light field in the angular domain remains a key challenge.

After obtaining geometric structural cues from the light field, the next crucial step is modeling temporal cues for light field object tracking. Over the past decades, various relational modeling methods have been proposed [6], [20]. These methods can be categorized into two classes: the first category directly connects adjacent frames and inputs them into neural networks, implicitly generating features that amalgamate motion and appearance information [21], [22]. The second category introduces appearance models, establishing contextual connections for images, and further utilizes temporal modules based on CNN or Transformer architectures to explicitly capture the temporal information in video sequences [23], [24]. While these methods have excelled in 2D object tracking tasks, they primarily focus on exploring spatio-temporal correlations based on dense pixel data. For sparse light field structural information, these methods might inadvertently aggregate some information from non-geometric structures of light field into the feature representation, thereby weakening the light field's ability to distinguish between targets and backgrounds. Thus, modeling temporal features of light fields requires not only consideration of inter-frame and intra-frame correlations in the angular domain but also effective aggregation of sparse geometric structural clues across angular-temporal dimensions. Additionally, current motion perception frameworks typically undergo supervised pre-training on large-scale video datasets [24], [5], followed by fine-tuning for downstream video tasks. However, due to the limited availability of light field datasets, relying solely on supervised learning is insufficient for effectively modeling the temporal features of light fields. Therefore, how to establish angular-temporal correlation for light field video and ensure effective learning is another key challenge.

To address the challenges mentioned above, this paper first proposes a novel representation for light fields, namely ESI. This representation explicitly delineates the geometric structure points within the light field by capitalizing on the abrupt changes in the angles of light rays within the epipolar plane, thereby enhancing the exploration of motion cues in the low-light scenes. We then propose an angular-temporal interaction

network (ATINet) for light field object tracking, designed to excavate rich discriminative features across angular-temporal dimensions. The proposed ATINet not only models inter-frame and intra-frame correlations in the angular domain but also efficiently gathers sparse geometric structure cues across angular-temporal dimensions through adaptive selection. Additionally, we introduce a self-supervised loss designed to optimize angular-aware representations for ATINet. This promotes interactions among geometric structural features in the temporal domain, thereby facilitating effective feature learning to support temporal matching. Next, we establish a large-scale benchmarks for light field single object tracking and multiple object tracking tasks, providing 173 and 26 light field videos respectively, each complete with bounding boxes and ESI representations. Finally, we evaluate the proposed ATINet on the light field single object tracking (SOT) task and extend the proposed method to the multiple object tracking (MOT) task with simple adjustments. Experimental results in these tasks showcase the competitive performance of our light field ATINet, affirming the effectiveness of our proposed method in low-light scenes. Our main contributions are:

- We propose a novel light field ESI representation that explicitly describes the geometric structure points within the light field by exploiting the abrupt properties of light rays within the epipolar plane, thereby enhance the expression of visual cues in low-light scenes. Compared to existing light field representations, the light field ESI removes high-dimensional redundant information and eliminates the need for designing complex angular modules.
- We introduce an angular-temporal interaction network (ATINet) for light field object tracking, which learns angular-aware representations from both geometric structural and angular-temporal interaction cues of light fields to address complex low-light scenes. Additionally, ATINet can be optimized using a self-supervised approach to improve the interaction of geometric features over the temporal domain.
- We construct a large-scale light field dataset for object tracking, comprising multiple complex objects carefully arranged in low-light scenes. Additionally, we validate the proposed method on light field SOT tasks and further extend it to MOT tasks, which have not been explored by previous methods. Extensive experiments demonstrate that our method achieves state-of-the-art performance on these tracking benchmarks.

II. RELATED WORK

A. Light Field for Computer Vision

Light field imaging captures light rays from various directions in a single shot, providing the captured image with both angular and spatial geometric structural information. This information in the light field contains various explicit and implicit scene cues, many of which have been widely used in computer vision tasks [14], [16]. Early work primarily focused on light field depth estimation [10], with several methods developed to exploit the distinctive spatio-angular information contained in the light field. These encompass occlusion-aware

techniques [11], considerations of photometric consistency [17], and EPI geometry modeling [25]. Recently, other visual tasks based on light fields have also garnered significant attention [12]. Zhang et al. [26] formulated the geometric coherence among multiple views in a light field as a graph. Through the effective utilization of a multi-scale graph neural network, they explored spatial complementary information and disparity correlation among multiple views in salient object detection. Meanwhile, Cong et al. [13] introduced a light field semantic segmentation network that efficiently fuses complementary information within the light field by utilizing supplementary features among different views. Furthermore, Wang et al. [19] proposed a light field single object tracking framework, which integrates the spatial-angular information of the light field into the appearance feature model to enhance tracking performance. Although considerable advancements have been made in computer vision for light fields, current research has not yet explored motion relation modeling, thereby limiting their generalizability to video scenarios. In this paper, we explicitly delineate geometric structure points by constructing a light field ESI and introduce an angular-temporal interaction network for light field video.

B. Object Tracking

Object tracking can be categorized into single object tracking (SOT) and multiple object tracking (MOT). SOT involves initializing the target's state in the first frame and tracking its subsequent movements. MOT aims to continuously track the trajectories of multiple targets across video frames. In the history of VOT, Discriminative Correlation Filters (DCF) emerged as the predominant paradigm [27]. Subsequent extensions of DCF-based trackers [28], [29] have consistently demonstrated excellent performance across multiple tracking benchmarks. With the advancement of deep learning, Siamese neural networks have emerged as a powerful tool in tracking. Bertinetto et al. [30] introduced SiamFC, designed to train the network from end to end. Building upon the foundation of SiamFC, researchers have conducted extensive studies, including backbone architectures [31], online model update [32], and target state estimation [33]. Furthermore, transformers have been employed in SOT and have garnered great attention [21], [22], [34]. These methods extract features through a single-stream or dual-stream encoder and utilize multi-head attention mechanisms to establish temporal correlations across multiple frames. For MOT, methods can be broadly classified into tracking-by-detection [5], [35] and joint detection and tracking [20], [23]. These strategies, equipped with detection information from the detector, excel at associating multiple objects within videos. Additionally, transformers have been employed in MOT [36], leveraging their capability to model interactions and dependencies among multiple targets, thereby enhancing tracking robustness in complex scenarios. Although SOT and MOT have achieved significant success, current methods that rely solely on appearance models experience performance degradation in low-light scenes. Our proposed model addresses this issue by effectively learning light field temporal cues, demonstrating its benefits in object tracking tasks.

C. Self-supervision Video Representation Learning

To circumvent the costly and time-intensive process of video data annotation, several self-supervised methods have been developed to extract video features from large-scale unlabeled videos [37], [38]. Self-supervised video representation learning trains neural networks using the objective functions of pretext tasks, leveraging the inherent structure of the data as a supervisory signal. Vondrick et al. [39] introduced a self-supervised learning method through video colorization to capture temporal information, leveraging the natural temporal consistency of colors to colorize grayscale videos by copying colors from reference frames. Meanwhile, Wang et al. [40] employed object motion tracking to learn video representations, and Goroshin et al. [41] utilized temporal coherence for the same purpose. Recently, inspired by the great success of self-supervised learning in NLP [42], masked image modeling (MIM) [7] have demonstrated promising results in video representation learning. Wu et al. [43] proposed adaptively performing spatial-attention dropout during frame reconstruction to facilitate the learning of temporal correspondences in videos. Sun et al. [44] captured long-term and fine-grained motion cues from sparse video inputs by reconstructing motion trajectories. Meanwhile, Gupta et al. [45] focused on object motion by maintaining the invariance of past frames while masking the majority of patches in future frames to learn object-centered representations. While such methods have demonstrated superior performance in 2D video, their application to learning light field video representation remains unexplored. In this paper, we constructed a light field self-supervised loss to extract angular-temporal features.

III. METHODS

This section introduces the light field EPI structure image (ESI), focusing on the extraction of geometric structural features to reduce light field redundancy. We then provide a detailed explanation of the proposed light field angular-temporal interaction network, which learns discriminative motion cues from the light field ESI stream. Lastly, we describe the training strategy and the expansion of the proposed method to other tasks.

A. Light Field Representation

The 4D light field, denoted as $L(u, v, x, y) \in \mathbb{R}^{U \times V \times W \times H}$ and represented by the two-plane model, can be transformed into alternative representations [14], [15], such as EPI images $\hat{L}_H(u, x) \in \mathbb{R}^{U \times W}$ or $\hat{L}_T(v, y) \in \mathbb{R}^{V \times H}$, as shown in Fig. 2(a-b). This representation with line structure attributes can be seamlessly integrated with traditional CNNs to extract intricate spatial-angular cues for scene understanding. While beneficial in some respects, the excessive redundancy of appearance information within EPI significantly hampers the light field's ability to express geometric structural properties in the angular domain. Effectively capturing the geometric structure of a light field in the angular domain is a key question.

Within a light field, the direction of light rays undergoes notable variations near the boundaries of objects due to their distinct refraction across different depth of field, as shown

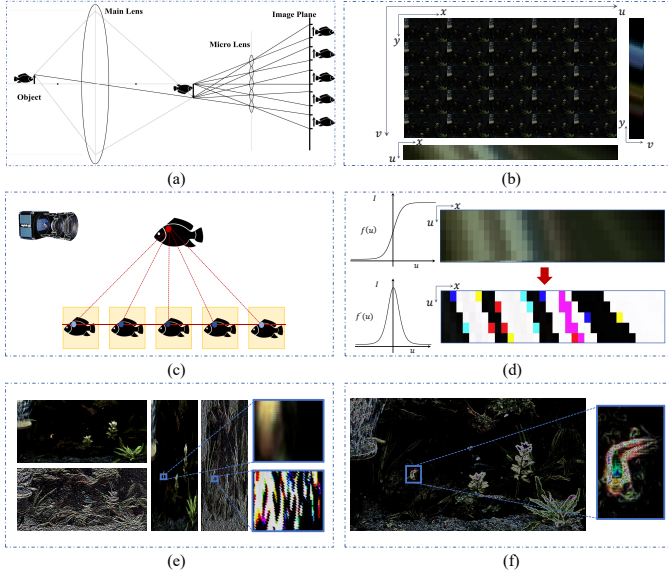


Fig. 2. Illustrations of light field representations: (a) Light field imaging system. (b) Light field multi-view and EPI representation. (c) Changes in viewpoints within the light field. (d) Calculation of geometric structure points. (e) Projection of all geometric structure points. (f) Generated light field ESI representation.

in Fig. 2(c). This phenomenon effectively delineates the geometric attributes of the light field. Consequently, this paper focuses on the abrupt changes of light rays, aiming to explicitly depict the geometric structure properties of the light field and eliminate unnecessary redundancy, thereby facilitating the exploration of temporal motion cues. Given that the directional properties of light rays are represented within the line structure of EPI, identifying locations with the maximum gradient in the angular dimension corresponds to pinpointing the spots where variations in light rays are most pronounced, as shown in Fig. 2(d). We name these specific points as geometric structure points within the light field. Based on the analysis above, we introduce a novel representation of light field, known as epipolar plane structure image (ESI). Next, we elucidate the construction process of ESI.

Given a candidate horizontal EPI image $\hat{L}_H(u, x)$ of $L(u, v, x, y)$, the gradient of a point along angular dimension can be described in conjunction with other viewpoints. That is, each EPI can reconstruct the geometric structure points through gradient computations. Specifically, for a horizontal EPI image, the gradient is formulated as follows:

$$\hat{L}'_u = [\alpha \hat{L}(u) + \beta \hat{L}(u + d_l) + \gamma \hat{L}(u + d_r)] + \eta_u \quad (1)$$

where d_l and d_r represent the left and right step sizes in the angular dimension, respectively. α, β, γ are coefficients, with η_u representing the consistency error. According to Taylor series expansion analysis, \hat{L}'_u can be approximated as follows:

$$\hat{L}'_u = \frac{d_r^2 \hat{L}(u + d_l) + (d_l^2 - d_r^2) \hat{L}(u + d_l) - d_l^2 \hat{L}(u - d_r)}{d_l d_r (d_l + d_r)} \quad (2)$$

Since the step size between angles in EPI is equal to the distance between adjacent micro-lens array centers (i.e., $d_l = d_r$),

can be simplified as:

$$\hat{L}'_u = \frac{\hat{L}(u + d) - \hat{L}(u - d)}{2d} \quad (3)$$

Here, we define $d = 1, u = U/2$, which detects abrupt changes in light rays based on the central view and its adjacent angular space. Therefore, we can search for geometric structure points by examining the first-order derivatives on all EPIs. Next, as shown in Fig. 2(e), we project these generated geometric structure points onto the plane to form horizontal EPI gradient image $S_H(x, u, y) \in \mathbb{R}^{W \times U \times H}$. Following the same method, the vertical EPI gradient image $S_T(v, x, y) \in \mathbb{R}^{V \times W \times H}$ can also be obtained. Finally, we calculate the amplitude of the horizontal and vertical EPI gradient images to form the final light field ESI, the process is formulated as follows:

$$S = \sqrt{S_H(u = U/2, x, y)^2 + S_T(v = V/2, x, y)^2} \quad (4)$$

The constructed light field ESI $S \in \mathbb{R}^{H \times W}$ is shown in Fig. 2(f). This representation explicitly delineates the geometric structure points within the light field by detecting the maximum values of the first-order derivatives in the angular space of the EPI. Therefore, we can observe that in low-light scenes, the light field ESI clearly represents the contours of the target.

B. Light Field Angular-Temporal Interaction Network

Learning discriminative motion cues from a light field ESI is challenging yet crucial for visual object tracking. Recent efforts in RGB streams have focused on modeling temporal relations by incorporating an attention-based module. Inspired by this, in this section, we introduce a light field angular-temporal interaction network (ATINet) for object tracking. The overall pipeline is shown in Fig. 3. The ATINet includes a dual-stream feature extraction process, where one stream inputs the ESI into the CNN backbone to generate appearance features for the template and search frames separately. The other stream inputs the ESI into our proposed light field angular-temporal modeling framework. The angular-temporal modeling framework consists of a feature extraction baseline and a proposed geometry adaptive selection method. After obtaining the feature maps from both streams, they are each processed through cross-correlation to form their respective correlation feature maps. Finally, we combine the correlation feature maps from both streams and input them into the tracking head. Next, we provide a detailed introduction to the feature extraction baseline and the proposed geometry adaptive selection method.

1) *Baseline*: The proposed baseline consists of multi-head attention (MHA) blocks and feed-forward networks (FFN). Specifically, we first randomly select two frames to construct a temporal pair $\{S^{t_1}, S^{t_2}\} \in \mathbb{R}^{H \times W \times 3}$ as input. Secondly, for the t_1 -th frame, S^{t_1} is divided into N non-overlapping patches of resolution $P \times P$, where $N = HW/P^2$. Thirdly, each of these patches undergoes a separate linear projection and is augmented with learnable position embeddings, resulting in light field patch embeddings $E^{t_1} \in \mathbb{R}^{N \times C}$, where C represents the embedding dimension. Following the same operations, we generate the embeddings for S^{t_2} , denoted as

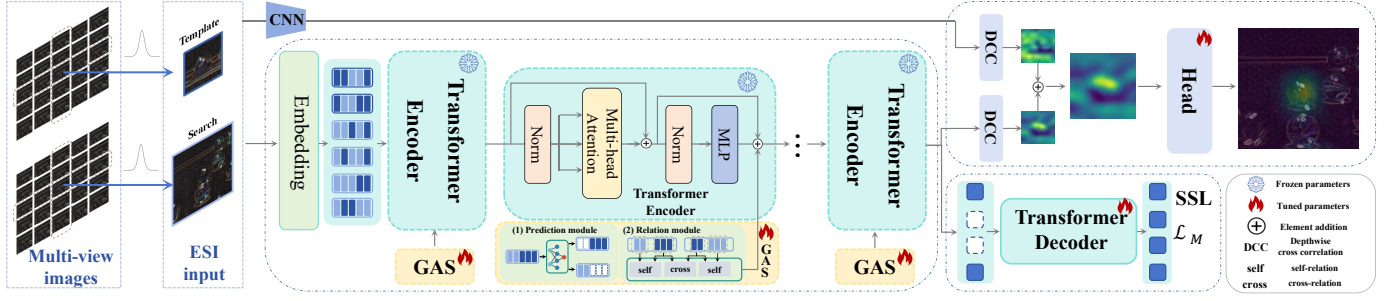


Fig. 3. An overview of our ATINet framework, which is a hybrid architecture tracker that employs Depthwise cross correlation to localize targets. It uses the ESI representation as input and integrates the proposed baseline with GAS as the feature extractor with a CNN backbone. During the training phase, only the GAS, the head networks, and decoder are fine-tuned. Additionally, the proposed SSL is used exclusively during the training phase.

$E^{t_2} \in \mathbb{R}^{N \times C}$. Afterward, we concatenate E^{t_1} and E^{t_2} to form a sequence with a length of $2N$, which is then fed into an encoder. In each encoder layer, input features are updated through MHA blocks and FFN. Formally, the process of the l -th encoder layer is:

$$[\hat{E}^{t_1}, \hat{E}^{t_2}]^l = [E^{t_1}, E^{t_2}]^l + \text{Att}([E^{t_1}, E^{t_2}]^l) \quad (5)$$

$$[E^{t_1}, E^{t_2}]^{l+1} = [\hat{E}^{t_1}, \hat{E}^{t_2}]^l + \text{FFN}([\hat{E}^{t_1}, \hat{E}^{t_2}]^l) \quad (6)$$

Since the multi-frame of the light field are jointly processed by multi-head self-attention blocks, and attention mechanisms can capture long-term dependency relationships, the modeling of cross-relations and self-relations is seamlessly integrated into each encoder layer. The output of self-attention operation can be defined as:

$$\text{Att}([E^{t_1}, E^{t_2}]) = \psi\left(\frac{[Q_{t_1}; Q_{t_2}][K_{t_1}; K_{t_2}]^T}{\sqrt{d_k}}\right)[V_{t_1}; V_{t_2}] \quad (7)$$

where ψ represents the softmax operation. Q , K , and V are query, key and value matrices of E^{t_1} and E^{t_2} . For multi-frame embeddings, the attention weights can be expanded to:

$$\frac{[Q_{t_1}; Q_{t_2}][K_{t_1}; K_{t_2}]^T}{\sqrt{d_k}} = \frac{[Q_{t_1} K_{t_1}^T, Q_{t_1} K_{t_2}^T, Q_{t_2} K_{t_1}^T, Q_{t_2} K_{t_2}^T]}{\sqrt{d_k}} \quad (8)$$

Therefore, the self-attention operation can be written as:

$$\text{Att}([E^{t_1}, E^{t_2}]) = \psi\left(\begin{bmatrix} \varphi(E^{t_1}, E^{t_1}) & \varphi(E^{t_1}, E^{t_2}) \\ \varphi(E^{t_2}, E^{t_1}) & \varphi(E^{t_2}, E^{t_2}) \end{bmatrix}\right) \begin{bmatrix} V_{t_1} \\ V_{t_2} \end{bmatrix} \quad (9)$$

where $\varphi(x, y) = Q_x K_y^T / \sqrt{d_k}$. In Eq. 9, the MHA block explores intra-frame features through self-relations in $\varphi(E^{t_1}, E^{t_1})$ and $\varphi(E^{t_2}, E^{t_2})$, simultaneously modeling inter-frame motion relationships through cross-relations in $\varphi(E^{t_1}, E^{t_2})$ and $\varphi(E^{t_2}, E^{t_1})$. Hence, the motion cues are effectively captured by the MHA block. Finally, the output of the last encoder layer is decoupled for two frames. These features are then reshaped into 2D feature maps based on their original positions, utilized for object tracking.

2) *Geometry Adaptive Selection*: Introducing the self-attention strategy into the baseline can effectively capture the angular cue correlations between multiple frames in the light field. However, for sparse light field ESI, this direct modeling may diminish feature representation, as certain features from non-geometric structure points can inadvertently aggregate

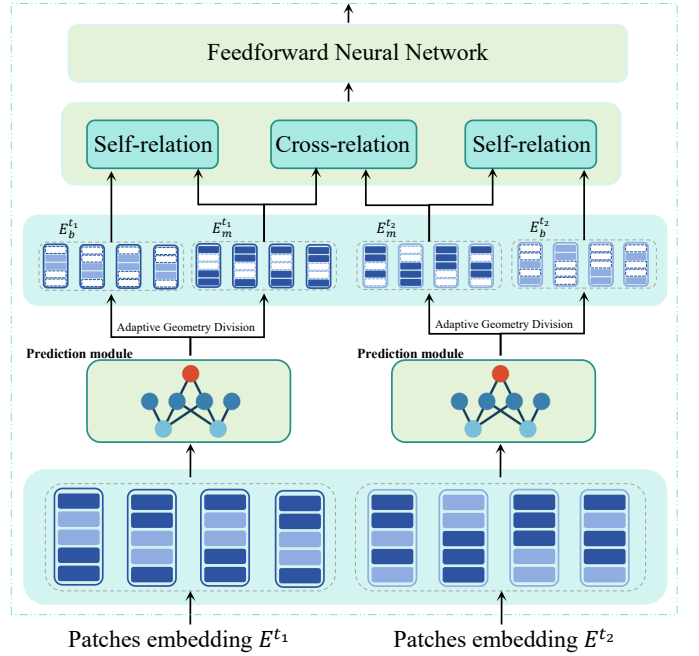


Fig. 4. An illustration of the geometry adaptive selection method. It is a plug-and-play module primarily divided into two steps. The first step involves adaptive geometric division using a prediction module. The second step establishes attentions between different embeddings, including self-relation and cross-relation.

into these representations, weakening the light field's capability for target-background recognition. To address this issue, we further introduce geometry adaptive selection (GAS) method, which adaptively selects geometric structure features for angular-temporal relation modeling. More specifically, our GAS consists of a lightweight multi-head attention block with an attached trainable prediction module. This module adaptively partitions the ESI embeddings into two groups: E_m and E_b , where E_m encapsulates the geometric structure point embeddings crucial for motion perception, while E_b encompasses the remaining non-geometric structure point embeddings. The prediction module can be formulated as:

$$\mathcal{P} = \psi_g(\text{MLP}([E^{t_1}, E^{t_2}])) \quad (10)$$

where MLP is a lightweight multi-layer perceptron and ψ_g is the Gumbel-Softmax. $\mathcal{P} \in \{0, 1\}^{2N \times 2}$, which is the one-hot tensor representing the labels of belonging to groups E_b and

E_m . Next, two columns of zeros are appended to the back of the sequence belonging to frame t_1 , and two columns of zeros are appended to the front of the sequence belonging to frame t_2 in \mathcal{P} . We denote the resulting tensors as $\hat{\mathcal{P}} \in \{0, 1\}^{2N \times 4}$, which indicate the labels of belonging to groups $E_b^{t_1}$, $E_m^{t_1}$, $E_b^{t_2}$ and $E_m^{t_2}$. Next, we construct a relation matrix using each column element of $\hat{\mathcal{P}}$. The process can be formulated as:

$$\mathcal{W}_{i,j} = \hat{\mathcal{P}}_{i,0}\hat{\mathcal{P}}_{j,0} + \hat{\mathcal{P}}_{i,1}(\hat{\mathcal{P}}_{j,1} + \hat{\mathcal{P}}_{j,3}) + \hat{\mathcal{P}}_{i,2}\hat{\mathcal{P}}_{j,2} + \hat{\mathcal{P}}_{i,3}(\hat{\mathcal{P}}_{j,3} + \hat{\mathcal{P}}_{j,1}) \quad (11)$$

where $\mathcal{W} \in \{0, 1\}^{2N \times 2N}$, the element $\mathcal{W}_{i,j}$ indicates whether the i -th embedding can model relations with the j -th embedding and aggregate information. It is noted that $\hat{\mathcal{P}}_{i,0}\hat{\mathcal{P}}_{j,0}$ and $\hat{\mathcal{P}}_{i,2}\hat{\mathcal{P}}_{j,2}$ represent self-relation modeling for the E_b groups of the two frames, without interacting with the E_m groups. $\hat{\mathcal{P}}_{i,1}(\hat{\mathcal{P}}_{j,1} + \hat{\mathcal{P}}_{j,3})$ and $\hat{\mathcal{P}}_{i,3}(\hat{\mathcal{P}}_{j,3} + \hat{\mathcal{P}}_{j,1})$ represent self-relation and cross-relation modeling for the E_m groups of the two frames. Afterward, we calculate the element-wise product of the relation matrix and the attention weight matrix to form the updated attention weight matrix. That is, $\psi_{i,j} \Rightarrow \mathcal{W}_{i,j} \cdot \psi_{i,j}$. Finally, the proposed GAS is integrated into each layer of the baseline. Therefore, Eq. (6) can be redefined as:

$$\begin{aligned} [E^{t_1}, E^{t_2}]^{l+1} &= F_{baseline} + GAS([E^{t_1}, E^{t_2}]^l) \\ F_{baseline} &= [\hat{E}^{t_1}, \hat{E}^{t_2}]^l + FFN([\hat{E}^{t_1}, \hat{E}^{t_2}]^l) \end{aligned} \quad (12)$$

It is worth noting that during the training phase, we only trained the GAS module, while the baseline parameters were from a pre-trained Vision Transformer (ViT), which has been proven to be effective in prompt learning [46]. In this way, the GAS can exclude non-geometric structure points and adaptively choose geometric structure points for angular-temporal relation modeling. This method facilitates the creation of discriminative representations for motion perception via the light field ESI.

C. Training Strategy and Task Expansion

Although ATINet has established temporal relations among geometric structure points in the light field, training it effectively remains a significant challenge. On one hand, achieving motion awareness in a light field necessitates unsupervised learning capabilities, akin to the human visual system's ability to establish visual correspondence over time. On the other hand, the limited availability of light field datasets requires GAS to focus more intensely on learning temporal relations. To address this challenge, we propose introducing a self-supervised loss (SSL) as the objective function for the light field. The loss function can be formulated as:

$$\mathcal{L}_M = \|\mathcal{D}_\phi(E \odot \mathcal{M}) - E \odot (1 - \mathcal{M})\|_2 \quad (13)$$

where \mathcal{M} represents a random mask designed to obscure a portion of the embedding features. The \odot symbol indicates element-wise product operation. $E = \mathcal{H}_{GAS}([E^{t_1}, E^{t_2}])$ and \mathcal{H}_{GAS} denotes the encoder network with the proposed GAS. \mathcal{D}_ϕ denotes the lightweight decoder network parameterized by ϕ , consisting of a small number of MHA blocks and FFN. Additionally, inspired by DropMAE [43], we introduce

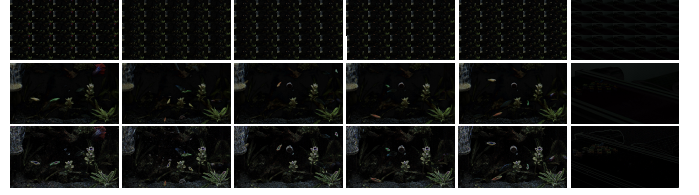


Fig. 5. Examples of light field tracking dataset. Top: The light field multi-view images. Bottom: The light field ESI representation.

adaptive spatial-attention dropout in \mathcal{D}_ϕ , which constrains interactions among embeddings of geometric structure points within the same frame in the decoder, while simultaneously encouraging more interactions with embeddings of geometric structure points from another frame. In this way, the proposed loss not only enables the training of network in an unsupervised manner but also encourages it to prioritize decoding using inter-frame cues. This compels the baseline with ATINet to focus on object motion for the effective learning of representations supporting temporal matching.

Finally, during the training phase, the total loss is formulated as follows:

$$\mathcal{L}_{total} = \lambda_1 \mathcal{L}_M + \lambda_2 \mathcal{L}_{cls} + \lambda_3 \mathcal{L}_{reg} \quad (14)$$

where λ_* is the weighting factor used to balance the training. The classification branch \mathcal{L}_{cls} is supervised using a Gaussian map generated from the ground truth center and employs focal loss, while the regression branch \mathcal{L}_{reg} is trained with IOU loss.

Furthermore, we develop a light field multiple object tracking framework (AMTrack) based on Trades [23]. Since Trades includes a cost volume-based association module to extract re-identification (re-ID) features and further match object similarities across frames, our AMTrack integrates GAS into the re-ID process and establishes a dual-stream re-ID layer to encode both appearance and geometric features. These features are combined for object association during tracking. Consistent with ATINet, the total loss for AMTrack is formulated as follows:

$$\mathcal{L}_{total} = \lambda_1 \mathcal{L}_M + \lambda_2 \mathcal{L}_{det} + \lambda_3 \mathcal{L}_{CVA} \quad (15)$$

where λ_* is the weighting factor used to balance the training. The \mathcal{L}_{det} represents the object detection loss. The CVA loss \mathcal{L}_{CVA} is supervised to learn an effective re-ID appearance embedding.

IV. EXPERIMENTS

A. Construction Datasets

Currently available light field datasets are based on static images and lack light field video data in real low-light scenarios. Therefore, we manually collect light field videos in low-light environments using the advanced Raytrix R8 camera [47]. The videos feature a diverse array of objects including glass spheres, toy cars, industrial nuts, and fish. Each scene is carefully composed of multiple, similar objects, creating a dynamic and complex motion flow within the video stream. Subsequently, we record these scenes using RxLive at a frame rate of 25 frames per second. RxLive captures

this data in a raw format as rays, which are then processed using the SDK interface of the Raytrix camera. Each light field frame undergoes parsing into multi-view images, which are further constructed into a light field ESI representation, as illustrated in Fig. 3. The spatial resolution of our light field is 1080×1920 , coupled with an angular resolution of 5×5 .

With the setup described above, we initially acquire over 12,500 light fields. Subsequently, we inspect the quality of each light field and discard samples with discrepancies. Following the filtering process, we retain 3,500 high-quality light fields, which ultimately form 26 light field video sequences, each containing approximately 150 frames. Next, we engage 30 participants to identify moving objects within each light field sequence. In accordance with the annotation standards of MOT16 [48], we assign a unique numerical identifier to each moving object within every video in the light field video series. Considering that each video contains 7 to 8 moving objects, this process results in the creation of the light field MOT dataset. Furthermore, we compile 160 objects exhibiting various movements from the light field MOT dataset and incorporate datasets of moving objects from other studies. This comprehensive effort results in the formation of the light field SOT dataset.

Finally, following the protocol established by MOT16, we divided the generated light field MOT datasets into training and testing subsets. The training subset contains 26 videos with 1,800 samples, and the testing subset includes an equivalent number of videos, totaling 1,500 samples. For the light field SOT dataset, we distributed the datasets into training and testing sets at a 6:4 ratio. The training set comprises 102 videos with 3,500 samples, whereas the testing set includes 71 videos, amassing 15,380 samples.

1) *Metrics*: To analyze the results of various methods in the SOT task, we employ three widely used evaluation metrics for quantitative performance assessment: precision, success, and normalized precision [49]. Additionally, we generate precision, normalized precision, and success plots for evaluation. For the MOT task, we utilize four evaluation metrics for performance assessment: false positives (FP) [50], false negatives (FN) [50], ID switches (IDS) [50], IDF1 [51], and Multiple Object Tracking Accuracy (MOTA) [50].

2) *Implementation Details*: We employ the PyTorch toolbox for our light field SOT and MOT tasks on a system equipped with four NVIDIA RTX 3090 GPUs. In the ATINet, our baseline is parameterized using a pre-trained ViT. The GAS module is integrated across all blocks of the baseline with settings of 12 layers depth, 16 attention heads, and an embedding dimension of 768. The mask rate in ALS is set at 0.5, and the decoder depth is set at 4. We optimize ATINet with a batch size of 96 for 25 epochs. For AMTrack, training spans 70 epochs with a maximum frame distance of 10, selecting 2 frames in total, and a training image size of 544×960 . During tracking, the detection and tracking thresholds are set at 0.5 and 0.4, respectively.

B. Comparisons with State-of-the-arts Methods

TABLE I
COMPARISON ON THE PROPOSED LIGHT FIELD TRACKING DATASET WITH HYBRID TRACKING FRAMEWORK. THE BEST RESULTS ARE MARKED IN BOLD.

Trackers	Years	Success \uparrow	Precision \uparrow	Norm.Prec. \uparrow
SiamRPN [52]	CVPR18	0.38	0.46	0.50
SiamRPN++ [53]	CVPR19	0.57	0.75	0.76
SiamDW [54]	CVPR19	0.44	0.55	0.58
ATOM [6]	CVPR19	0.42	0.49	0.50
DiMP [29]	ICCV19	0.59	0.71	0.72
SiamFC++ [55]	AAAI20	0.57	0.74	0.76
PrDiMP [28]	CVPR20	0.57	0.68	0.69
SiamCAR [56]	CVPR21	0.55	0.74	0.76
SiamAPN [57]	ICRA21	0.45	0.65	0.68
STMTrack [58]	CVPR21	0.55	0.70	0.71
LFTrack [19]	TII23	0.36	0.46	0.51
STARK [59]	ICCV21	0.57	0.67	0.68
OSTrack [21]	ECCV22	0.59	0.71	0.71
SimTrack [60]	ECCV22	0.61	0.74	0.75
MixFormerV2 [61]	NeurIPS23	0.53	0.64	0.66
ZoomTrack [62]	NeurIPS23	0.61	0.73	0.74
ATINet	-	0.64	0.79	0.81

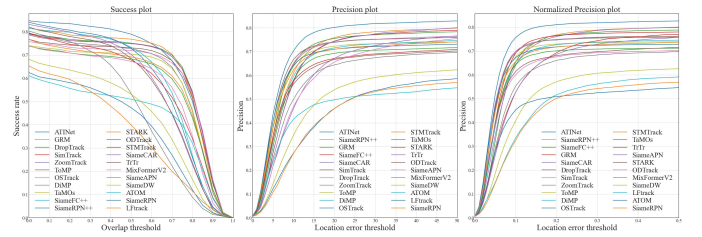


Fig. 6. Overall performance of all trackers.



Fig. 7. Visual comparison of different trackers. The first and second rows depict the results of hybrid trackers, with the black box indicating ground truth, the red box representing our tracker, the blue box indicating DiMP, and the white box representing SiamFC++. The third and fourth rows showcase the results of pure transformer trackers, with the same color scheme used to denote ground truth, our tracker, DropTrack, and OSTrack, respectively.

1) *Evaluation for Single Object Tracking*: As the state-of-the-art in the light field ESI domain remains largely unexplored, we conduct a comprehensive evaluation of our proposed method by comparing it with 16 existing state-of-the-art methods on light field ESI datasets. Specifically, our competitors include 11 hybrid methods: ATOM [6], DiMP [29], PrDiMP [28], SiamRPN [52], SiamRPN++ [53], SiamDW [54], SiamFC++ [55], SiamCAR [56], STMTrack [58], SiamAPN [57], and LFTrack [19]; and 5 pure transformer methods: STARK [59], OSTrack [21], SimTrack [60], MixFormerV2 [61], and ZoomTrack [62]. Notably, LFTrack

TABLE II
QUANTITATIVE COMPARISON OF THE STATE-OF-THE-ART METHODS ON THE LFMOT DATASET.

Model	Years	MOTA \uparrow	IDF1 \uparrow	IDS \downarrow	FP \downarrow	FN \downarrow
CenterTrack [20]	ECCV20	87.1	71.2	339	626	2029
Trades [23]	CVPR21	87.3	83.3	123	416	2394
ByteTrack [5]	ECCV22	74.2	81.2	66	2770	3140
Hybrid-SORT [35]	AAAI24	85.3	75.3	201	310	2904
AMTrack	-	87.5	85.4	125	455	2306

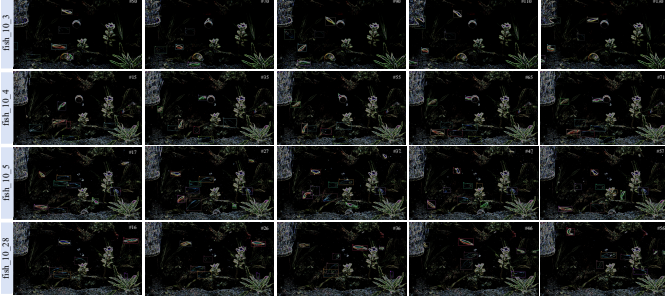


Fig. 8. Visual tracking results of the proposed light field MOT algorithm on some scenes.

also employs light field-based tracking. For a fair comparison, we re-train these trackers on our training dataset using their default parameter settings, rather than directly testing them on the testing subset.

The quantitative results are listed in Table I, where we observe that our method outperforms the other methods, with higher success and precision. This is primarily because trackers are generally optimized for RGB image tracking and struggle with processing and modeling features from light field ESI inputs, particularly in low-light scenes. Furthermore, these trackers tend to focus predominantly on spatial dimension information extraction, neglecting the angular-temporal dimension. This oversight leads to their inability to leverage visual motion cues within light field videos effectively. Owing to the specialized design of our GAS tailored for light field ESI, integrating it into tracking framework significantly enhances performance compared to other methods. Additionally, we visualize the performance curves in Fig. 6, which demonstrate the potential of light field motion cues in SOT. By learning geometric structural cues in the angular-temporal dimensions, our method can effectively extract light field motion features to accurately localize targets in low-light scenes.

To observe the visual quality of the tracking results produced by our method and others, we present several representative examples in Fig. 7. Although recent RGB imaging-based methods have made significant progress, they still fall short in exploiting the geometric structural information of light fields to accurately locate moving targets in low-light scenes, particularly those involving targets like fish that exhibit significant deformations, similarity interference, and motion blur. In contrast, our method successfully distinguishes moving objects in these complex scenes, demonstrating the superiority of our proposed method in light field tracking.

2) *Evaluation for Multiple Object Tracking*: To fully evaluate the performance of our method in the light field MOT task,

TABLE III
ABLATION STUDY FOR KEY COMPONENTS.

	ESI	GAS	SSL	Success \uparrow	Precision \uparrow	Norm.Prec. \uparrow
1				0.58	0.74	0.76
2	✓			0.59	0.73	0.74
3	✓	✓		0.62	0.77	0.78
4	✓		✓	0.60	0.75	0.77
5	✓	✓	✓	0.64	0.79	0.81

we compared our proposed method with four other state-of-the-art MOT methods that use light field ESI as input. These methods include CenterTrack [20], Trades [23], ByteTrack [5], and Hybrid-SORT [35]. To ensure a fair comparison, we retrained these trackers using their default parameter settings on our training dataset.

Table II presents a comparison between our proposed MOT method and other algorithms. As indicated in Table II, our method achieved the highest MOTA score among these state-of-the-art methods. This underscores the superior overall performance of our proposed method compared to competing algorithms. Additionally, our method also recorded the highest IDF1 score among all methods compared, demonstrating its exceptional capability in maintaining long-term tracking of consistent target trajectories. Moreover, by incorporating temporal motion information from the light field, our algorithm increasingly concentrates on time-series-related objects. This enhancement allows the tracker to accurately match most objects, which exhibit comparatively low miss detection rates.

Fig. 8 illustrates several frames of tracking results generated by our method. The consistency of the estimated trajectories is indicated by bounding boxes marked with identical colors and ID numbers. From the figure, it is evident that our method can successfully locate and identify most objects within complex low-light environments. These results not only confirm that the light field ESI effectively captures complex object information for MOT tasks, but also highlight that our proposed method is adept at accurately learning re-identification embedding information crucial for tracking associations.

C. Ablation Study and Analysis

To explore the benefits of different design choices in the proposed ATINet, we conduct thorough ablation studies in this section.

1) *Effectiveness of Key Components*: In this subsection, we conduct ablation studies to assess the significance of various components. The performance of various methods is displayed in Table III. The first row illustrates the baseline results, which do not incorporate light field components and instead use the single view of the light field as the direct input. This row shows lower performance metrics, suggesting that basic spatial cues alone are inadequate for fully capturing the motion states of objects in complex low-light scenes. In the second row, we incorporate the proposed light field ESI as input. However, we observe no significant enhancement in tracker performance. This is mainly due to traditional feature modeling methods being ineffective at extracting the sparse

TABLE IV
ABLATION STUDY FOR DIFFERENT ESI REPRESENTATION.

	Input	Success \uparrow	Precision \uparrow	Norm.Prec. \uparrow
1	ESI _{Max}	0.56	0.70	0.71
3	ESI _{Mean}	0.56	0.71	0.73
4	ESI _{Sum}	0.57	0.73	0.74
5	ESI _V	0.59	0.74	0.75
6	ESI _H	0.58	0.73	0.75
7	ESI	0.64	0.79	0.81

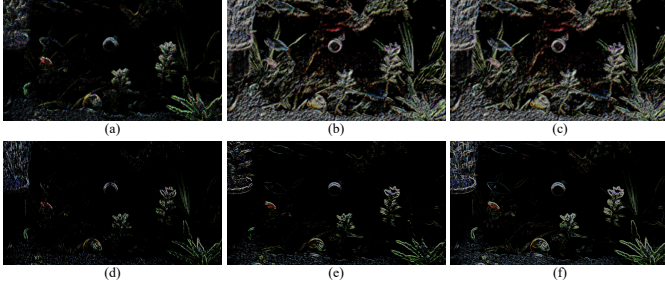


Fig. 9. Visual results of different light field representations. (a) ESI_{max}. (b) ESI_{mean}. (c) ESI_{sum}. (d) ESI_H. (e) ESI_V. (f) ESI.

structured cues inherent in ESI. In contrast, the third row introduces GAS, which specifically focuses on light field angular-temporal modeling, allowing the tracker to better comprehend complex scenes. Meanwhile, in the fourth row, our proposed SSL significantly enhances the model’s training efficiency on limited datasets. Finally, in the fifth row, by integrating all three proposed light field components, the tracker achieves an optimal configuration, thereby validating the effectiveness of our approach.

2) *Analysis on Different ESI Representation:* In our proposed ESI, we select the gradient values from the central view ($u = U/2$) and calculate the amplitude of the horizontal and vertical EPI gradient images to form the final light field ESI representation. In this subsection, we explore various light field representations by adopting alternative settings. Specifically, we capture the maximum, mean, and sum values across the u and v dimensions from the horizontal and vertical EPI gradient images, defining these as ESI_{max}, ESI_{mean}, and ESI_{sum}. Additionally, we directly calculate the amplitude of the horizontal and vertical EPI gradient images to establish directional representations from a single viewpoint, designated as ESI_H and ESI_V. As shown in Table IV, the metrics confirm that the ESI representation significantly improves performance. The statistically derived ESI_{mean} and ESI_{sum} representations struggle with continuity in edge regions, as depicted in Fig. 9. Moreover, the unidirectional ESI_H and ESI_V representations fail to capture significant changes in light field targets. Conversely, the proposed ESI can capture the geometric structure and motion of the target across both horizontal and vertical directions, thereby achieving optimal results.

3) *Analysis on Different GAS Setting:* In the proposed GAS, GAS is embedded into all layer of neurons in the baseline model. In this subsection, we assess the effectiveness of GAS in light field angular-temporal modeling by selectively

TABLE V
ABLATION STUDY FOR DIFFERENT SETTINGS WITH THE PROPOSED GAS.

	Type	Success \uparrow	Precision \uparrow	Norm.Prec. \uparrow
1	baseline	0.60	0.75	0.77
2	GAS _{shallow}	0.63	0.79	0.80
3	GAS _{depth}	0.62	0.78	0.78
4	GAS _{intra}	0.59	0.74	0.76
5	GAS _{inter}	0.61	0.76	0.78
6	GAS	0.64	0.79	0.81

TABLE VI
THE COMPUTATIONAL COMPLEXITY ANALYSIS IN THE NETWORKS WITH OR WITHOUT THE PROPOSED GAS.

Type	FLOPs \downarrow	Params \downarrow	Time \downarrow
baseline	39.07	99.78	0.019 \pm 0.0001
baseline+SSL	39.44	100.77	0.053 \pm 0.0003
baseline+GAS+SSL (Ours)	44.35	113.31	0.066 \pm 0.0010

removing GAS branches from the deep and shallow layers of our method. Additionally, we modify the configuration of the relation matrix within the GAS branches to evaluate the efficacy of our relational modeling. The results are presented in Table 5. Specifically, GAS_{depth} and GAS_{shallow} refer to the integration of GAS into the deep and shallow layers of the baseline, respectively. GAS_{intra} and GAS_{inter} represent the modeling of only intra-frame and inter-frame correlations, respectively, within the E_m groups for two frames. Compared to GAS_{depth} and GAS_{shallow}, our method shows significant improvements. The comparison results confirm the effectiveness of our proposed GAS module in the both deep and shallow layers. Additionally, our method outperforms both GAS_{intra} and GAS_{inter}. This indicates that angular-temporal modeling for light fields must consider not only the temporal correlations across frames but also the intra-frame structural correlations.

4) *Analysis of Computational Complexity:* The main computational demand of our light field ATINet arises from the prediction module in GAS and the calculation of relationship matrices, as well as the decoder part in SSL. To assess the complexity of our method, we compare the computational complexity of the network embedded with GAS and SSL to that of the original network. Results in Table VI showcase the parameters, FLOPs, and inference time for networks with and without GAS and SSL. It is evident from Table VI that, our SSL does not incur additional parameter costs due to its lightweight decoding design. Furthermore, as a plug-and-play module, our GAS introduces only a minimal computational load to the original network. Consequently, when our method is integrated into downstream tasks, there is merely a slight increase in computational complexity.

V. CONCLUSION

In this paper, we observe that the geometric structure within the light field is effectively represented by abrupt changes in the angular domain. Inspired by this observation, we propose a succinct light field ESI representation. This representation aims to reduce redundancy in high-dimensional light fields

and enhance the expression of visual cues in low-light scenes. To learn angular-aware representations from the geometric structure and angular-temporal interaction cues of the light field, especially in complex low-light scenes, we introduce an angular-temporal interaction network (ATINet) for light field object tracking, which includes multiple GAS modules and an SSL mechanism. The GAS module selectively gathers sparse geometric structure cues across angular-temporal dimensions and models the correlations within and between frames in the angular domain. The SSL optimizes light field angular-temporal learning through a self-supervised manner, further enhancing the interaction of geometric features across the temporal domain. Additionally, we establish a large-scale light field video benchmark, providing significant data support for light field SOT and light field MOT tasks. Our experiments validate the effectiveness of our proposed methods and report state-of-the-art results on these two representative visual tasks. Furthermore, through analysis and comparison of various modules, the experiments show that our proposed method is feasible and effective for achieving target-level temporal matching tasks in low-light scenes. In the future, we plan to extend our approach to more advanced pixel-level visual tasks.

ACKNOWLEDGMENTS

This work was supported by National Natural Science Foundation of China (NSFC) (62272342, 62020106004), and Tianjin Natural Science Foundation (23JCJC00070). The 2022 Tianjin Research and Innovation Project under grant number 2022BKJY160, and Tianjin University of Technology 2022 Post-graduate Research and Innovation Practice Project under grant number YJ2238.

REFERENCES

- [1] J. Jin, M. Guo, J. Hou, H. Liu, and H. Xiong, "Light field reconstruction via deep adaptive fusion of hybrid lenses," *IEEE Transactions on Pattern Analysis and Machine Intelligence*, 2023.
- [2] Y. Wang, L. Wang, G. Wu, J. Yang, W. An, J. Yu, and Y. Guo, "Disentangling light fields for super-resolution and disparity estimation," *IEEE Transactions on Pattern Analysis and Machine Intelligence*, vol. 45, no. 1, pp. 425–443, 2022.
- [3] W. Gao, S. Fan, G. Li, and W. Lin, "A thorough benchmark and a new model for light field saliency detection," *IEEE Transactions on Pattern Analysis and Machine Intelligence*, 2023.
- [4] X. Wei, Y. Bai, Y. Zheng, D. Shi, and Y. Gong, "Autoregressive visual tracking," in *Proceedings of the IEEE/CVF Conference on Computer Vision and Pattern Recognition*, 2023, pp. 9697–9706.
- [5] Y. Zhang, P. Sun, Y. Jiang, D. Yu, F. Weng, Z. Yuan, P. Luo, W. Liu, and X. Wang, "Bytetrack: Multi-object tracking by associating every detection box," in *European conference on computer vision*. Springer, 2022, pp. 1–21.
- [6] M. Danelljan, G. Bhat, F. S. Khan, and M. Felsberg, "Atom: Accurate tracking by overlap maximization," in *Proceedings of the IEEE/CVF conference on computer vision and pattern recognition*, 2019, pp. 4660–4669.
- [7] K. He, X. Chen, S. Xie, Y. Li, P. Dollár, and R. Girshick, "Masked autoencoders are scalable vision learners," in *2022 IEEE/CVF Conference on Computer Vision and Pattern Recognition (CVPR)*, 2022, pp. 15 979–15 988.
- [8] Q. Qu, X. Chen, Y. Y. Chung, and W. Cai, "Lfacon: introducing anglewise attention to no-reference quality assessment in light field space," *IEEE Transactions on Visualization and Computer Graphics*, vol. 29, no. 5, pp. 2239–2248, 2023.
- [9] Y. Chen, G. Jiang, M. Yu, H. Xu, and Y.-S. Ho, "Deep light field spatial super-resolution using heterogeneous imaging," *IEEE Transactions on Visualization and Computer Graphics*, 2022.
- [10] Y. Wang, L. Wang, G. Wu, J. Yang, W. An, J. Yu, and Y. Guo, "Disentangling light fields for super-resolution and disparity estimation," *IEEE Transactions on Pattern Analysis and Machine Intelligence*, vol. 45, no. 1, pp. 425–443, 2022.
- [11] M. Strecke, A. Alperovich, and B. Goldluecke, "Accurate depth and normal maps from occlusion-aware focal stack symmetry," in *Proceedings of the IEEE Conference on Computer Vision and Pattern Recognition*, 2017, pp. 2814–2822.
- [12] M. Wang, F. Shi, X. Cheng, M. Zhao, Y. Zhang, C. Jia, W. Tian, and S. Chen, "Lfbnet: Light field boundary-aware and cascaded interaction network for salient object detection," in *Proceedings of the 30th ACM International Conference on Multimedia*, 2022, pp. 3430–3439.
- [13] R. Cong, D. Yang, R. Chen, S. Wang, Z. Cui, and H. Sheng, "Combining implicit-explicit view correlation for light field semantic segmentation," in *Proceedings of the IEEE/CVF Conference on Computer Vision and Pattern Recognition*, 2023, pp. 9172–9181.
- [14] P. Li, J. Zhao, J. Wu, C. Deng, Y. Han, H. Wang, and T. Yu, "Opal: Occlusion pattern aware loss for unsupervised light field disparity estimation," *IEEE Transactions on Pattern Analysis and Machine Intelligence*, 2023.
- [15] W. Zhou, L. Lin, Y. Hong, Q. Li, X. Shen, and E. E. Kuruoglu, "Beyond photometric consistency: Geometry-based occlusion-aware unsupervised light field disparity estimation," *IEEE Transactions on Neural Networks and Learning Systems*, 2023.
- [16] K. Han, W. Xiang, E. Wang, and T. Huang, "A novel occlusion-aware vote cost for light field depth estimation," *IEEE Transactions on Pattern Analysis and Machine Intelligence*, vol. 44, no. 11, pp. 8022–8035, 2021.
- [17] M. W. T. P. P. Srinivasan, S. H. S. Rusinkiewicz, and J. M. R. Ramamoorthi, "Shape estimation from shading, defocus, and correspondence using light-field angular coherence," *IEEE Transactions on Pattern Analysis and Machine Intelligence*, vol. 39, no. 3, 2017.
- [18] J. Zhang, Y. Liu, S. Zhang, R. Poppe, and M. Wang, "Light field saliency detection with deep convolutional networks," *IEEE Transactions on Image Processing*, vol. 29, pp. 4421–4434, 2020.
- [19] M. Wang, F. Shi, X. Cheng, M. Zhao, Y. Zhang, C. Jia, W. Tian, and S. Chen, "Visual object tracking based on light-field imaging in the presence of similar distractors," *IEEE Transactions on Industrial Informatics*, vol. 19, no. 3, pp. 2705–2716, 2022.
- [20] X. Zhou, V. Koltun, and P. Krähenbühl, "Tracking objects as points," in *European conference on computer vision*. Springer, 2020, pp. 474–490.
- [21] B. Ye, H. Chang, B. Ma, S. Shan, and X. Chen, "Joint feature learning and relation modeling for tracking: A one-stream framework," in *European Conference on Computer Vision*. Springer, 2022, pp. 341–357.
- [22] Y. Cui, C. Jiang, L. Wang, and G. Wu, "Mixformer: End-to-end tracking with iterative mixed attention," in *Proceedings of the IEEE/CVF Conference on Computer Vision and Pattern Recognition*, 2022, pp. 13 608–13 618.
- [23] J. Wu, J. Cao, L. Song, Y. Wang, M. Yang, and J. Yuan, "Track to detect and segment: An online multi-object tracker," in *Proceedings of the IEEE/CVF conference on computer vision and pattern recognition*, 2021, pp. 12 352–12 361.
- [24] C. Mayer, M. Danelljan, G. Bhat, M. Paul, D. P. Paudel, F. Yu, and L. Van Gool, "Transforming model prediction for tracking," in *Proceedings of the IEEE/CVF conference on computer vision and pattern recognition*, 2022, pp. 8731–8740.
- [25] Y. Zhang, H. Lv, Y. Liu, H. Wang, X. Wang, Q. Huang, X. Xiang, and Q. Dai, "Light-field depth estimation via epipolar plane image analysis and locally linear embedding," *IEEE Transactions on Circuits and Systems for Video Technology*, vol. 27, no. 4, pp. 739–747, 2016.
- [26] Q. Zhang, S. Wang, X. Wang, Z. Sun, S. Kwong, and J. Jiang, "Geometry auxiliary salient object detection for light fields via graph neural networks," *IEEE Transactions on Image Processing*, vol. 30, pp. 7578–7592, 2021.
- [27] M. Danelljan, G. Bhat, F. Shahbaz Khan, and M. Felsberg, "Eco: Efficient convolution operators for tracking," in *Proceedings of the IEEE conference on computer vision and pattern recognition*, 2017, pp. 6638–6646.
- [28] M. Danelljan, L. V. Gool, and R. Timofte, "Probabilistic regression for visual tracking," in *Proceedings of the IEEE/CVF conference on computer vision and pattern recognition*, 2020, pp. 7183–7192.
- [29] G. Bhat, M. Danelljan, L. V. Gool, and R. Timofte, "Learning discriminative model prediction for tracking," in *Proceedings of the IEEE/CVF international conference on computer vision*, 2019, pp. 6182–6191.
- [30] L. Bertinetto, J. Valmadre, J. F. Henriques, A. Vedaldi, and P. H. Torr, "Fully-convolutional siamese networks for object tracking," in *Computer Vision—ECCV 2016 Workshops: Amsterdam, The Netherlands, October*

- 8-10 and 15-16, 2016, *Proceedings, Part II 14*. Springer, 2016, pp. 850–865.
- [31] B. Li, W. Wu, Q. Wang, F. Zhang, J. Xing, and J. Yan, “Siamrpn++: Evolution of siamese visual tracking with very deep networks,” in *Proceedings of the IEEE/CVF conference on computer vision and pattern recognition*, 2019, pp. 4282–4291.
 - [32] L. Zhang, A. Gonzalez-Garcia, J. V. D. Weijer, M. Danelljan, and F. S. Khan, “Learning the model update for siamese trackers,” in *Proceedings of the IEEE/CVF international conference on computer vision*, 2019, pp. 4010–4019.
 - [33] N. Wang, W. Zhou, Y. Song, C. Ma, W. Liu, and H. Li, “Unsupervised deep representation learning for real-time tracking,” *International Journal of Computer Vision*, vol. 129, pp. 400–418, 2021.
 - [34] L. Lin, H. Fan, Z. Zhang, Y. Xu, and H. Ling, “Swintrack: A simple and strong baseline for transformer tracking,” *Advances in Neural Information Processing Systems*, vol. 35, pp. 16 743–16 754, 2022.
 - [35] M. Yang, G. Han, B. Yan, W. Zhang, J. Qi, H. Lu, and D. Wang, “Hybrid-sort: Weak cues matter for online multi-object tracking,” in *Proceedings of the AAAI Conference on Artificial Intelligence*, vol. 38, no. 7, 2024, pp. 6504–6512.
 - [36] F. Zeng, B. Dong, Y. Zhang, T. Wang, X. Zhang, and Y. Wei, “Motr: End-to-end multiple-object tracking with transformer,” in *European Conference on Computer Vision*. Springer, 2022, pp. 659–675.
 - [37] J. Wang, J. Jiao, L. Bao, S. He, W. Liu, and Y.-h. Liu, “Self-supervised video representation learning by uncovering spatio-temporal statistics,” *IEEE Transactions on Pattern Analysis and Machine Intelligence*, vol. 44, no. 7, pp. 3791–3806, 2022.
 - [38] L. Jing and Y. Tian, “Self-supervised visual feature learning with deep neural networks: A survey,” *IEEE Transactions on Pattern Analysis and Machine Intelligence*, vol. 43, no. 11, pp. 4037–4058, 2021.
 - [39] C. Vondrick, A. Shrivastava, A. Fathi, S. Guadarrama, and K. Murphy, “Tracking emerges by colorizing videos,” in *Proceedings of the European conference on computer vision (ECCV)*, 2018, pp. 391–408.
 - [40] X. Wang and A. Gupta, “Unsupervised learning of visual representations using videos,” in *Proceedings of the IEEE international conference on computer vision*, 2015, pp. 2794–2802.
 - [41] R. Goroshin, J. Bruna, J. Tompson, D. Eigen, and Y. LeCun, “Unsupervised learning of spatiotemporally coherent metrics,” in *Proceedings of the IEEE international conference on computer vision*, 2015, pp. 4086–4093.
 - [42] J. Devlin, M.-W. Chang, K. Lee, and K. Toutanova, “Bert: Pre-training of deep bidirectional transformers for language understanding,” in *North American Chapter of the Association for Computational Linguistics*, 2019. [Online]. Available: <https://api.semanticscholar.org/CorpusID:52967399>
 - [43] Q. Wu, T. Yang, Z. Liu, B. Wu, Y. Shan, and A. B. Chan, “Dropmae: Masked autoencoders with spatial-attention dropout for tracking tasks,” in *Proceedings of the IEEE/CVF Conference on Computer Vision and Pattern Recognition*, 2023, pp. 14 561–14 571.
 - [44] X. Sun, P. Chen, L. Chen, C. Li, T. H. Li, M. Tan, and C. Gan, “Masked motion encoding for self-supervised video representation learning,” in *Proceedings of the IEEE/CVF Conference on Computer Vision and Pattern Recognition*, 2023, pp. 2235–2245.
 - [45] A. Gupta, J. Wu, J. Deng, and L. Fei-Fei, “Siamese masked autoencoders,” *arXiv preprint arXiv:2305.14344*, 2023.
 - [46] W. Liu, X. Shen, C.-M. Pun, and X. Cun, “Explicit visual prompting for low-level structure segmentations,” in *Proceedings of the IEEE/CVF Conference on Computer Vision and Pattern Recognition*, 2023, pp. 19 434–19 445.
 - [47] “Raytrix gmbh.” <https://raytrix.de/>. Accessed:2019-02-03.
 - [48] A. Milan, L. Leal-Taixé, I. Reid, S. Roth, and K. Schindler, “Mot16: A benchmark for multi-object tracking,” *arXiv preprint arXiv:1603.00831*, 2016.
 - [49] Y. Wu, J. Lim, and M. Yang, “Online object tracking: A benchmark,” in *2013 IEEE Conference on Computer Vision and Pattern Recognition*, 2013, pp. 2411–2418.
 - [50] K. Bernardin and R. Stiefelhagen, “Evaluating multiple object tracking performance: the clear mot metrics,” *EURASIP Journal on Image and Video Processing*, vol. 2008, pp. 1–10, 2008.
 - [51] E. Ristani, F. Solera, R. Zou, R. Cucchiara, and C. Tomasi, “Performance measures and a data set for multi-target, multi-camera tracking,” in *European conference on computer vision*. Springer, 2016, pp. 17–35.
 - [52] B. Li, J. Yan, W. Wu, Z. Zhu, and X. Hu, “High performance visual tracking with siamese region proposal network,” in *Proceedings of the IEEE conference on computer vision and pattern recognition*, 2018, pp. 8971–8980.
 - [53] B. Li, W. Wu, Q. Wang, F. Zhang, J. Xing, and J. Yan, “Siamrpn++: Evolution of siamese visual tracking with very deep networks,” in *Proceedings of the IEEE/CVF conference on computer vision and pattern recognition*, 2019, pp. 4282–4291.
 - [54] Z. Zhang and H. Peng, “Deeper and wider siamese networks for real-time visual tracking,” in *Proceedings of the IEEE/CVF conference on computer vision and pattern recognition*, 2019, pp. 4591–4600.
 - [55] Y. Xu, Z. Wang, Z. Li, Y. Yuan, and G. Yu, “Siamfc++: Towards robust and accurate visual tracking with target estimation guidelines,” in *Proceedings of the AAAI conference on artificial intelligence*, vol. 34, no. 07, 2020, pp. 12 549–12 556.
 - [56] D. Guo, J. Wang, Y. Cui, Z. Wang, and S. Chen, “Siamcar: Siamese fully convolutional classification and regression for visual tracking,” in *Proceedings of the IEEE/CVF conference on computer vision and pattern recognition*, 2020, pp. 6269–6277.
 - [57] C. Fu, Z. Cao, Y. Li, J. Ye, and C. Feng, “Siamese anchor proposal network for high-speed aerial tracking,” in *2021 IEEE International Conference on Robotics and Automation (ICRA)*. IEEE, 2021, pp. 510–516.
 - [58] Z. Fu, Q. Liu, Z. Fu, and Y. Wang, “Stmtrack: Template-free visual tracking with space-time memory networks,” in *Proceedings of the IEEE/CVF conference on computer vision and pattern recognition*, 2021, pp. 13 774–13 783.
 - [59] B. Yan, H. Peng, J. Fu, D. Wang, and H. Lu, “Learning spatio-temporal transformer for visual tracking,” in *Proceedings of the IEEE/CVF international conference on computer vision*, 2021, pp. 10 448–10 457.
 - [60] B. Chen, P. Li, L. Bai, L. Qiao, Q. Shen, B. Li, W. Gan, W. Wu, and W. Ouyang, “Backbone is all your need: A simplified architecture for visual object tracking,” in *European Conference on Computer Vision*. Springer, 2022, pp. 375–392.
 - [61] Y. Cui, T. Song, G. Wu, and L. Wang, “Mixformerv2: Efficient fully transformer tracking,” *Advances in Neural Information Processing Systems*, vol. 36, 2024.
 - [62] Y. Kou, J. Gao, B. Li, G. Wang, W. Hu, Y. Wang, and L. Li, “Zoom-track: Target-aware non-uniform resizing for efficient visual tracking,” *Advances in Neural Information Processing Systems*, vol. 36, 2024.